

Central Lancashire Online Knowledge (CLoK)

Title	Simple Size Tuning of Magnetic Nanoparticles using a Microwave Solvothermal Method and their Application to Facilitate Solid Phase Synthesis of Smart Polymers.
Type	Article
URL	https://clok.uclan.ac.uk/id/eprint/54512/
DOI	https://doi.org/10.1039/D4MA01115E
Date	2025
Citation	Stephen, Andrei Nino, Mercer, Tim, Stockburn, William, Dennison, Sarah Rachel, Readman, Jennifer Elizabeth and Reddy, Subrayal M orcid iconORCID: 0000-0002-7362-184X (2025) Simple Size Tuning of Magnetic Nanoparticles using a Microwave Solvothermal Method and their Application to Facilitate Solid Phase Synthesis of Smart Polymers. Materials Advances.
Creators	Stephen, Andrei Nino, Mercer, Tim, Stockburn, William, Dennison, Sarah Rachel, Readman, Jennifer Elizabeth and Reddy, Subrayal M

It is advisable to refer to the publisher's version if you intend to cite from the work. https://doi.org/10.1039/D4MA01115E

For information about Research at UCLan please go to http://www.uclan.ac.uk/research/

All outputs in CLoK are protected by Intellectual Property Rights law, including Copyright law. Copyright, IPR and Moral Rights for the works on this site are retained by the individual authors and/or other copyright owners. Terms and conditions for use of this material are defined in the http://clok.uclan.ac.uk/policies/



Materials Advances



Accepted Manuscript

This article can be cited before page numbers have been issued, to do this please use: A. N. Stephen, T. Mercer, W. J. Stockburn, S. Dennison, J. Readman and S. M. Reddy, *Mater. Adv.*, 2025, DOI: 10.1039/D4MA01115E.



This is an Accepted Manuscript, which has been through the Royal Society of Chemistry peer review process and has been accepted for publication.

Accepted Manuscripts are published online shortly after acceptance, before technical editing, formatting and proof reading. Using this free service, authors can make their results available to the community, in citable form, before we publish the edited article. We will replace this Accepted Manuscript with the edited and formatted Advance Article as soon as it is available.

You can find more information about Accepted Manuscripts in the <u>Information for Authors</u>.

Please note that technical editing may introduce minor changes to the text and/or graphics, which may alter content. The journal's standard <u>Terms & Conditions</u> and the <u>Ethical guidelines</u> still apply. In no event shall the Royal Society of Chemistry be held responsible for any errors or omissions in this Accepted Manuscript or any consequences arising from the use of any information it contains.



13

14

15

16 17

18

19 20

21

22

23

24

25

26 27

28

29

30

31

32 33

34

35

39

- 1 Simple Size Tuning of Magnetic Nanoparticles using a Microwave MA01115E
- 2 Solvothermal Method and their Application to Facilitate Solid Phase
- 3 Synthesis of Smart Polymers.
- 4 Andrei N Stephen¹, Tim Mercer², William Stockburn¹, Sarah R Dennison¹, Jennifer E Readman¹
- 5 and Subrayal M Reddy^{1*}
- 6 ¹Department of Chemistry, Institute of Materials and Investigative Sciences, UCLan Centre for
- 7 Smart Materials, School of Pharmacy and Biomedical Sciences, University of Central
- 8 Lancashire, Preston, PR1 2HE, United Kingdom.
- 9 ²Magnetic Materials Research Group, Jeremiah Horrocks Institute for Mathematics, Physics &
- 10 Astronomy, University of Central Lancashire, Preston, PR1 2HE.
- 11 *Corresponding author: smreddy@uclan.ac.uk

Abstract

We demonstrate a simple, economical, rapid and scalable microwave method to produce magnetite-based magnetic nanoparticles (MNPs) at a desired size and their application to facile synthesis of high value polymer products. One solvothermal method gaining traction is the use of microwave synthesis as it offers a rapid and green method to MNP production. In this work, we report a previously unreported simple and reliable microwave synthesis method where adjusting the temperature gradient from 20 °C to a dwell temperature of 200 °C produces size control of superparamagnetic aldehyde functionalised nanoparticles (MNP@CHO). Nanoparticles size distributions measured using dynamic light scattering range from for 14 nm ±8 nm at 90 °C/min (a 2-minute ramp time to dwell temperature) and 122 nm ± 49 nm at 18 °C/min (a 10-minute ramp time to dwell temperature) and are produced within 20-30 minutes. Magnetic sizing analysis using the method of Chantrell confirmed iron-oxide core size increases as a function of ramp time over the range 7.91 to 11.25 nm in terms of median diameter and with lognormal σ values within (0.22 $\leq \sigma \leq$ 0.33). Particle cluster size increase with increasing ramp time measured using transmission electron microscopy was found to be a function of particle agglomeration. Further, we demonstrate that the MNP@CHO functionalised with a protein of interest can then be applied to the rational solid phase synthesis of molecularly imprinted polymer nanoparticles (nanoMIPs) with high affinity for protein biomarkers. We demonstrate that there is an optimal MNP size for highly efficient MNP-based nanoMIP production which is key to mass production and commercialisation of low-cost and sustainable bespoke size-tuned MNPs and artificial antibodies.

Keywords:

magnetic nanoparticles; MNP; IONP; SPION; size control; superparamagnetism; microwave synthesis; solid-phase polymer synthesis; molecularly imprinted polymers; MIPs; electrochemical; biosensors

41

42

43

44

45 46

47

48

49

50

Highlights	View Article Online DOI: 10.1039/D4MA01115E

- Simple size-tuning of MNPs by altering the microwave synthesis temperature gradient prior to reaching dwell time.
- The method facilitates uniformity and surface functionalization in a single step.
- Clustering is encouraged by increasing the temperature ramping time
- Demonstration that size affects properties in the application of functionalised MNPs for the solid phase synthesis of nanoscale smart polymers (MIPs)

52

53

54

55

58

59

60

61

62

63

64 65

66

67 68

69 70

71

72

73

74

75

76

77

78 79

80

81 82

83

84

85

86 87

88

89

90

91 92

View Article Online Introduction DOI: 10.1039/D4MA01115E

Magnetite (Fe₃O₄)-based magnetic nanoparticles (MNPs) also referred to as iron oxide nanoparticles (IONPs) continue to receive a lot of attention, both in research and commercial applications 1-3. Fe₃O₄ is preferred over other nanomaterials due to the relatively low toxicity of magnetite ⁴⁻⁶ as well as the ready availability and low cost of the reaction precursors ^{6, 7}. Their ability to be superparamagnetic 7, 8 has enabled this wide range of applications of

56

57 superparamagnetic iron oxide nanoparticles (SPIONs).

For superparamagnetism (SPM) to occur, magnetite particles are typically considered at sizes smaller than about 20 nm 8-10; however it should be noted that the SPM onset size is affected by a number of factors, including shape effects on anisotropy and the particle size distribution present in any assembly of SPIONS, such that it may be observed at sizes up to $\sim 50 \text{ nm}^{11, 12}$ Unlike the ferrimagnetic behaviour of the bulk material, at these small sizes the particles demonstrate superparamagnetic properties with no net magnetisation in zero applied field 8. In this state, the particle magnetic moments are randomly aligned by at room temperature by the agitation of thermal energy and hence show no magnetic interaction with each other (similar to paramagnets), whereas in a magnetic field, superparamagnetic nanoparticles exhibit significantly increased magnetization due to the ready alignment of moments with the applied field. Their ability to be easily moved and manipulated by an external magnetic field due to their superparamagnetic properties, is providing a range of applications in the biomedical field including targeted anti-cancer drug delivery ¹³, as MRI contrasting agents ¹⁴-¹⁶, for biological extraction/purification when functionalised with suitable receptors ^{17, 18}, for cancer treatment under magnetic hyperthermia conditions¹⁹⁻²², and more recently in the molecularly imprinting field²³.

A range of approaches have been explored using low-cost reagents. The main methods have focused on producing Fe₃O₄ nanoparticle clusters using coprecipitation,²⁴⁻²⁷ solvothermal²⁸⁻ ³¹, and hydrothermal^{32, 33} reactions. Traditional co-precipitation methods, are generally rapid but require the use of inert gases like argon and nitrogen to prevent the creation of other, less useful iron oxides, maintaining the correct iron oxidation states³⁴⁻³⁷. They also require an additional step to neutralize the resultant solution requiring strong bases such as urea and sodium hydroxide, which increases the cost of the process. Furthermore, to achieve an adequate level of size control, additional equipment, such as magnetic arrays³⁸ and ultrasonicators³⁹, are necessary. These requirements make scaling up far more challenging.

Hydrothermal methods involve the reaction of iron precursors in sealed specialized vessels⁴⁰, ⁴¹ to autoclave under high-temperature and high-pressure aqueous conditions over the course of a lengthy 6-20 hours⁴², typically with the aid of stabilizing agents or surfactants. The hydrothermal environment promotes nucleation and growth of iron oxide nanocrystals, leading to highly uniform and monodisperse particles as shown in Mizutani et al.43 Among them, solvothermal reactions offer the best monodispersity, typically utilizing diethylene glycol (DEG) and ethylene glycol (EG) as a reducing solvent, sodium citrate tribasic as a ligand, and a basic salt such as sodium acetate (NaOAc). The above method typically takes 8 hrs to synthesise and to subsequently functionalise and a further 24 hrs to purify the resulting MNPs. 31 The conventional heating provides large temperature gradients leading to variable

96 97

98

99

100 101

102

103

104

105106

107 108

109 110

111

112113

114

115

116 117

118

119

120121

122

123

124

125

126

127

128

129

130131

132

133

134135

nucleation rates, but the obtained particles can be produced with narrow size distribution. Additional particles can be produced with narrow size distribution. Which is albeit over a much longer timescale to product compared with microwave methods.

Microwave synthesis of magnetic nanoparticles offers a simplified production process with reduced costs compared to traditional methods, while also presenting significant environmental advantages, making it a more sustainable and greener alternative⁴⁴⁻⁴⁶. Traditional co-precipitation methods often necessitate inert atmospheres such as argon or nitrogen to prevent oxidation during synthesis, which increases energy demands and environmental impact⁴⁷⁻⁴⁹. Conversely, microwave synthesis can be performed under ambient conditions, eliminating the need for inert gases and thereby reducing the overall carbon footprint of the process. Furthermore, co-precipitation and hydrothermal methods typically require extended heating durations, often lasting several hours, to synthesize magnetic nanoparticles, leading to considerable energy consumption⁵⁰. Microwave synthesis, on the other hand, is inherently more energy-efficient due to its rapid and localized heating mechanism, which enables nanoparticle formation within an hour or less, drastically minimizing energy input. The one-pot nature of our microwave synthesis also reduces the need for additional reagents or multi-step processing due to the fact that the magnetic nanoparticles are formed with a coating though the microwave synthesis process⁴⁶, further lowering waste generation. Unlike co precipitation and hydrothermal methods relying on coatings after the synthesis⁵¹ adding extra cost and complexity or the addition of additives to provide size control. our microwave synthesis enables precise size control through simple adjustments in ramping parameters, generating less chemical waste. Overall, microwave synthesis of magnetic nanoparticles represents a greener and more sustainable alternative to conventional techniques. By reducing energy consumption, avoiding the use of inert gases, and minimizing waste, this approach aligns with modern environmental sustainability goals while efficiently delivering high-quality nanoparticles.

Microwave heating offers more controlled and homogeneous heating throughout the medium resulting in reproducible syntheses of colloidal materials. Microwave-based one-pot solvothermal synthesis of bare and functionalized superparamagnetic Fe₃O₄ MNPs in the <20 nm category is gaining traction as it offers a low energy and rapid (<30 min) route to product⁴⁶. While small MNPs (<15 nm) can be useful, they are prone to drag fluctuations due to Brownian motion even under the influence of a magnetic field ⁵². There have been recent reports of synthesis of larger MNP clusters composed of smaller superparamagnetic nanoparticles⁵³⁻⁵⁵. With these methods, larger particles (25 nm to approximately 1 μ m) are possible, this increase in size scale offering advantageous applications compared with the smaller regime. An increase in MNP volume to surface area (ie production of a lower concentration of such larger agglomerated particles) enables the chemical functionalization (conjugation) of more than one molecule or biomolecule to each MNP allowing for an increase in capture of more than one complementary molecule per MNP from a sample of interest, while still retaining superparamagnetic properties⁵⁶.

Methods to predictably control the size of MNPs within a batch-type synthesis, while not altering other properties, remains highly desirable. As the size increases, the nanoparticles become less superparamagnetic, but the magnetic saturation becomes greater⁵⁷. Magnetic saturation is one of the most important properties when considering applications based on

137

138

139

140

141

142

143144

145

146

147

148

149

150

151 152

153154

155

156

157 158

159

160161

162163

164

165

166

167168

169

170171

172

173174

175

176

177

178

magnetic nanoparticles⁵⁸ ⁵⁹. A high magnetic saturation leads to a strong response at a magnetic field which can, for example, facilitate the rapid collection of analytes when they are used for biological extraction and biosensing. Moreover, for imaging, the strong response results in much more sharply defined images^{60, 61}. Therefore, by having a method that can tune the size over a range, one can increase saturation magnetisation while still maintaining superparamagnetic properties.

There have been reports of tuning the sizes of nanoparticle clusters by for example adjusting the ratio of DEG/EG^{62, 63}, and adjusting the citrate concentration⁶². However, these methods do not yet offer fine control over the final particle size without affecting monodispersity or other parameters, such as composition and yield, and offer only a limited tuning range. The use of polyol solvents in microwave-assisted techniques offers several advantages beyond their reducing capabilities. In the polyol method, diethylene glycol (DEG) and ethylene glycol (EG) function not only as solvents and reducing agents but also as surfactants and are chosen for their relative high dielectric constants, which enable efficient microwave absorption and heating⁶⁴. Mascolo et al. ⁶⁵ have demonstrated a size tuning in magnetite clusters through simple stoichiometric (chemical) control of reaction solution basicity in the presence of a cationic surfactant and at room temperature. An excess concentration of OH⁻ led to the stabilisation of smaller particles (<10 nm). The aggregate particle size (ranging 40 to 100 nm) could be increased by decreasing the hydroxide concentration. Others⁶⁶⁻⁶⁸ have used microfluidics and flow chemistry to control the rate at which the reaction solution transits a microwave reactor to control the size of synthesised iron oxide nanoparticles and associated clusters. The method required significant engineering to control the size and volume of the micro/milli-fluidic reactor used, minimise laminar flow and the need for scaling up synthesis at speed. Our microwave synthesis method is inherently scalable and well-suited to industrial applications, given the availability of industrial-scale microwave reactors. Unlike conventional co-precipitation or hydrothermal methods, our microwave method requires no additional specialized equipment, thereby eliminating the need for complex fabrication and testing processes.

In this paper, we focus on tuning the physical conditions and parameters used in microwave synthesis as a means to control the final MNP nanoparticle size. We report an approach to control and tune the size of aldehyde functionalised iron oxide magnetic nanoparticles and their clustering by simply changing the microwave temperature gradient during MNP synthesis. We investigate sizing using dynamic light scattering, transmission electron microscopy and magnetometry. The magnetic materials produced have a hydrodynamic diameter ranging 36 nm to 122 nm measured using dynamic light scattering. We propose a mechanism where with change in temperature ramp time, there is an accompanying change in rate of decomposition of an iron acetate intermediate in the reaction as the route to tune the MNP entity size. We also propose that oligomerisation and integration of glutaraldehyde during the MNP growth phase contributes to the formation of uniform MNP cluster sizes. The proposed method not only tunes particle size but also facilitates uniformity and surface functionalization in a single step.

More recently aldehyde functionalised MNPs have been applied to the synthesis of artificial antibody receptors, namely nanoscale molecularly imprinted polymers (NanoMIPs) ^{23, 69}. MIPs

Open Access Article. Published on 11 February 2025. Downloaded on 2/14/2025 1:59:45 PM.

This article is licensed under a Creative Commons Attribution 3.0 Unported Licence.

are produced in a facile self-assembly and polymerisation process in the presence of a target include Molitist template molecule. When the template is removed, polymeric materials with high affinity for the target are produced. Suitably functionalised MNPs have been used as the nucleation site for nanoMIP production. The MNPs have also been modified with sometimes esoteric chemistry using silanisation of the MNP surface^{70, 71} or use of borane chemistry ^{72, 73} and subsequent bioconjugation with a template molecule to enable nanoMIP synthesis at the MNP surface. While these methodologies have resulted in the production of high affinity nanoMIPs, they have been laborious, time-consuming (up to 3 days) and reagent heavy for production ultimately resulting in low (milligram) yields. We recently published a solid phase synthesis method using microwave produced aldehyde MNPs as core for protein (template) attachment and subsequent production of nanoMIPs ²³. We present in this paper the application of size-tuned nanoMIPs and demonstrating that MNP size is critical to optimising yields of high affinity nanoMIPs.

2. Experimental

2.1 Materials

N-hydroxymethylacrylamide (NHMA, 48% w/v), N,N'-methylenebisacrylamide (MBAm; 99% pure), ethylene glycol((CH2OH)2; 99% pure), iron chloride (FeCl3·6H2O; 96% pure), methylhydroquinone (MHQ; 99% pure), sodium acetate (NaOAc; \geq 99% pure), phosphate buffered saline tablets (PBS, 10 mM, pH 7.4 \pm 0.2), potassium ferricyanide (K3Fe(CN)6;99% pure), potassium chloride (KCl;99% pure), sodium nitrate (NaNO3; \geq 99% pure), ammonium persulphate (APS; 98% pure), N,N,N',N' -tetramethylethylenediamine (TEMED; 99% pure), potassium peroxydisulfate (KPS; \geq 99% pure (RT)), haemoglobin from bovine blood (BHb), bovine serum albumin (BSA), sodium dodecyl sulphate (SDS; \geq 98.5% pure) and glutaraldehyde (25% v/v)) were used as received from Merck. Buffers were prepared in MilliQ water (resistivity 18.2 \pm 0.2 M Ω .cm). DropSens disposable screen-printed electrodes (Au-BT) comprising a gold working electrode (0.4 cm diameter), a platinum counter electrode and silver reference electrode were purchased from Metrohm (Runcorn, Cheshire, UK). **2.2**

Instrumentation

BioDrop μ LITE UV/visible spectrometer was purchased from Biochrom Ltd Cambridge, UK. Nicolet AVATAR 330 FTIR spectrophotometer with Pike MIRacle accessory and FEI Tecnai 12 TEM at 100 kV with a Tietz F214 2k × 2k CCD camera were purchased from Thermo Fisher Scientific, Loughborough, UK. Anton Paar monowave 200 microwave oven was purchased from Anton Paar Ltd Hertfordshire, UK. SLS Lab basics centrifuge was purchased from Scientific Laboratory Supplies, Nottingham, UK. All electrochemical experiments were performed using a Metrohm Autolab PGSTAT204 potentiostat and NOVA2.1.4 software. Magnetisation curves were obtained using a 6 kOe Vibrating Sample Magnetometer (VSM) built in-house at UCLan.

View Article Online

DOI: 10.1039/D4MA01115E

2.3 MNP Production using Microwave Synthesis

Bare and aldehyde functionalised magnetic particles were produced following our previously published solvothermal microwave method ²⁰. Briefly, 0.5 g of FeCl₃·6H₂O and 1.8 g of NaOAc were dissolved in 15 mL of ethylene glycol in a 30 mL Anton Parr G30 microwave reaction vial (MRV). Glutaraldehyde (3.5 mL) was then added to the resulting solution with stirring for a further 5 min. The stirrer bar was then removed and the MRV was placed into an Anton Paar monowave 200 microwave oven and the reaction was heated up to a dwell temperature of 200 °C. We investigated various ramp times to dwell temperature from slow ramp time (10 mins; 18 °C/min) and fast ramp time (2 mins; 90 °C/min). The reaction was held at the dwell temperature for 20 min under pressure (9 bar). An aliquot (10mL) of the MNP suspension was oven dried (110 °C for 2 days) for use in TEM analysis. The MNP production method was repeated, but in the absence of gluataraldehyde, to give bare MNPs.

2.4 X-ray diffraction analysis

X-ray powder diffraction data were collected using a Bruker D2 Phaser diffractometer in θ - θ geometry, using Cu K α radiation (λ = 1.5418 Å) and operating at 30 keV and 30 mA. A nickel filter was used to remove K β radiation and a LynxEye detector. Data were collected between 5 – 80° 2-theta, with a step size of 0.020194° and a total scan time of 1 hour per sample. The energy discrimination of the detector was modified to surpress fluorescence from the iron containing samples. The sample holder was rotated at 30 rpm to maximise powder averaging. Crystallite size analysis was performed using the Bruker EVA software. The peak width of the peak at approximately 35.5° 2-theta was measured at FWHM and used in the Scherrer calculation.

2.5 DLS characterization of MNPs

The size distribution of the nanoparticles was characterized using a Zetasizer Nano ZS. The produced MNPs/nanoMIPS/NanoNIPs were suspended in 1 mL of PBS. The sample was loaded into a disposable cuvette with the refractive index set to 1.32. The solution was equilibrated for 60 seconds before the measurement was taken. Measurements were formed in triplicate.

2.6 Magnetic Measurements

Magnetic Measurements on dried powder samples were carried out at a room temperature using a 6 kOe Vibrating Sample Magnetometer (VSM). As large agglomerates are formed by drying, a pestle and mortar was required to break them up for packing into cuboid glass slides (Camlab) of given internal thickness and width of (0.40 + 0.04) mm and (4.0 + 0.4) mm respectively. The slides were cut at ~ 10 mm in length within the range (9.75 \geq length \geq 11.60) mm resulting in errors of the order 10^{-2} mm from a minimum of 5 measurements along the length at different points across the width. From these dimensions, the magnetometric demagnetisation factors, N_d , were found to be low and in the range (0.037 \geq N_d \geq 0.044) 74

2.7 Transmission Electron Microscopy of MNPs

View Article Online DOI: 10.1039/D4MA01115E

Aldehyde functionalized MNPs were suspended in ultra-pure water (0.1 g in 50 μ l water) and a 5 μ l droplet was deposited onto a Formvar/carbon coated 200 mesh copper TEM grid (Agar Scientific, UK). After 1 min the grid was blotted, washed for 30 s in ultra-pure water, blotted again and allowed to dry. Images were collected using a FEI Tecnai 12 TEM at 100 kV with a Tietz F214 2k × 2k CCD camera.

264

265

266

267268

269

270271

272273

274

275

276277

278279

280

281

282

283

284

285

286

287

288

289290

291

292

293

294

295296

297

258

259

260

261

262

263

2.8 Protein Functionalization of MNPs

A suspension (1 mL) equivalent to 0.010 g of the produced aldehyde (-CHO) functionalised magnetic nanoparticle (MNP@CHO; 10 mg/mL) was placed in an Eppendorf centrifuge tube. A neodymium magnet was placed on the side of the tube to rapidly pull the magnetic nanoparticles from the solution (10 minutes). The supernatant was removed and replaced with 1 mL of a 1 mg/mL PBS solution of bovine haemoglobin (BHb). The Eppendorf was then sonicated for 2 minutes followed by vigorous shaking and vortexing to ensure the nanoparticles were fully dispersed. The reaction mixture was left undisturbed at room temperature (22 °C) for 30 minutes allowing the protein to conjugate with the MNP@CHO. Conjugation occurs due to free -NH2 groups in the protein undergoing a nucleophilic additionelimination reaction with -CHO on MNP resulting in a imine bond between protein and MNP. After 30 minutes, the particles were once again separated from the solution and the supernatant exchanged with fresh buffer in triplicate to remove any non-conjugated protein. The amount of protein conjugated with the MNPs (functionalized and bare) was calculated through comparing the initial and final concentrations of protein remaining in the supernatant. The concentration of the non-adsorbed protein was measured by spectrophotometry (405 nm for haemoglobin) using a BioDrop µLITE UV/visible spectrometer. The resulting MNP@CHO@BHb particles thus produced were stored wet at 4 °C until further use.

2.9 NanoMIP production using MNPs

The MNP@CHO@BHb magnetic nanoparticles (0.023 g) were resuspended in 906 μ L of PBS (pH7.4) and transferred to a 15mL falcon tube. The tube was then mixed at 400 rpm at room temperature. The sample was then degassed using nitrogen for 15 minutes with stirring. The nitrogen line was then removed and 37 mg of NHMA monomer (77 μ L of 48% v/v solution) and MBAm (6 mg) together with SDS (0.4 mg) were immediately added to the reaction mixture, followed by 20 μ L of a solution containing 20% (v/v) TEMED and 10% (w/v) APS. A nitrogen headspace was then created, and the falcon tube sealed with the cap and then wrapped in parafilm. The solution was left to mix at 400 rpm for 15 minutes to allow nanoMIP particles to be produced at the surface of the MNP@CHO@BHb particles.

At 15 minutes, the reaction was rapidly quenched with 1mL of 10 mM methylhydroquinone (MHQ) The reaction solution was exchanged three times with fresh PBS to remove any unreacted monomers and quencher. The solution was then resealed, and the tube placed on its side on a neodymium magnet (2 minutes). The supernatant was then removed. The

305

306

307

308

309

310

311

312

313 314

315

316 317

318 319

320

321

322

323

324

325

326

327

332

333

334 335

336

MNP@CHO@BHb~nanoMIP particles were then dispersed in 600 μL of e-pure water MAO1115E 298 299 placed in a sonicator (using a VWR ultrasonicator (600W, 45kHz) for 5 minutes at 37 °C. The falcon tube was then once again placed on a neodymium magnet and the supernatant now 300 containing the released nanoMIPs were placed in a 1.5 mL volume Eppendorf and stored at 4 301 °C until further use. The preparation was repeated by using either bare MNP and MNP@CHO 302 instead of MNP@CHO@BHb to produce non-imprinted control polymer (nanoNIP). 303

2.10 Electrochemical Deposition and Analysis of NanoMIP

NanoMIPs were eluted using sonication and were then entrapped within an electropolymerized layer (E-layer). E-Layers were fabricated directly onto BT-Au screenprinted electrodes (SPEs; Metrohm) using cyclic voltammetry (CV) largely following the procedure in ⁷⁵. Briefly, a 50 µL solution in PBS comprising 0.1 mg of nanoMIP, 1.33 M of NHMA as the functional monomer, 41.5 mM MBAm as the cross-linker, 0.29 M NaNO₃, 48.15 mM KPS was deposited onto the SPE. The potential was then cycled between -0.2 V and -1.4 V for 7 cycles at 50 mV s⁻¹ (10 min, RT, 22 ±2 °C) to produce the E-layer with entrapped nanoMIP. E-layers in the absence of nanoMIP were also produced as a control.

The E-layer comprising entrapped nanoMIP islands (E-NMI) or control E-layer were exposed to varying concentrations of target protein (haemoglobin) template solutions over a wide concentration range (1 fM to 100 µM) for a period of 5 minutes at each concentration and analysed using electrochemical impedance spectroscopy (EIS) post-rebinding and subsequent rinsing in order to determine the degree of target rebound to the nanoMIP islands.

Selective protein binding was tracked using electrochemical impedance spectroscopy (EIS) of an external 5 mM potassium ferricyanide solution in PBS containing 0.5 M KCl as supporting electrolyte. Electrochemical impedance spectroscopy (EIS) measurements were conducted at a standard potential of 0.1 V (± 0.01 V) with 10 scans of frequencies, and a sinusoidal potential peak-to-peak with amplitude 0.01 V in the 0.1 - 100000 Hz frequency range. A Randles equivalent circuit was fitted for all EIS experiments using the FRA32 module (see Supplementary Fig. 1).

3. Results and Discussion

3.1 Characterisation of MNPs Produced using the Microwave Technique.

We have previously reported 46 our microwave synthesis method for rapid production of 328 magnetic nanoparticles where the temperature gradient from 20 °C to 200 °C was fixed at 90 329 330 $^{\circ}\text{C}$ /min (representing a 2 minute ramp time), resulting in MNPs with an average size of 7 \pm 2

331 nm, measured using transmission electron microscopy.

In this paper, we varied the time taken to reach the dwell temperature (200 °C). We investigated ramp times of 2, 4, 6, 8, 10 and 15 minutes corresponding to temperature gradients of 90, 45, 30, 22.5, 18 and 12 °C/min respectively. This resulted in the production of aldehyde functionalised magnetic nanoparticles (MNP@CHO). Particle in dispersion ranging 14 nm to 120 nm were measured using dynamic light scattering spectroscopy as summarised in Fig 1 (See Supplementary Figs. S1(a-e)). Particles produced at a ramp time of $\frac{1}{2}$ min had the consistency of an oily slurry and could not be easily dispersed in aqueous solution. DLS analysis indicated that the average particle size was in the 1-2 μ m range. Additionally, these particles produced at a ramp time of 15 min were no longer susceptible to an external magnetic field using a neodymium magnet.

342

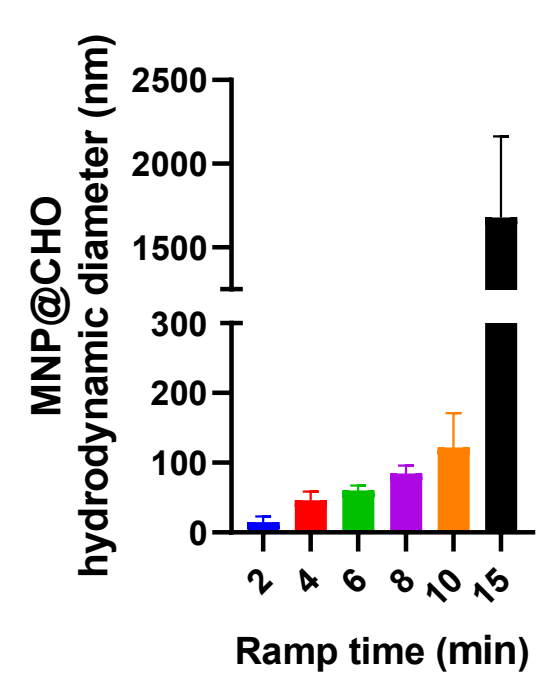
337

338

339

340

341



343344

Fig. 1 Effect of microwave temperature ramp time from room temperature to dwell temperature (200 $^{\circ}$ C) on size of final MNP@CHO nanoparticles. Hydrodynamic diameter of particles measured using dynamic light spectroscopy. (Data represents mean \pm S.E.M., n = 3)

347

345

346

We propose that the difference in particle size is related to the rate at which reactants are consumed as a function of ramp time (Fig. 2).

Ethylene glycol is primarily solvent, but can act as a mild reducing agent resulting in the production of Fe^{2+} ions en route to producing Fe_3O_4 according to the following equations ⁷⁶:

$$352 2HOCH_2 - CH_2OH \rightarrow 2CH_3CHO + 2H_2O (1)$$

$$353 2CH_3CHO + 2Fe^{3+} \rightarrow CH_3CO - COCH_3 + 2Fe^{2+} + 2H^+ (2)$$

$$354 2Fe^{2+} + 40H^{-} \rightleftharpoons 2Fe(0H)_{2} (3)$$

$$355 4Fe(OH)_3 + 2Fe(OH)_2 \rightarrow 2Fe_3O_4 + 8H_2O (4)$$

Acetate is included to prevent particle agglomeration during MNP synthesis⁷⁷. Lt. aid MAO1115E 358 production of Fe(OH)₃ and subsequently maghemite and magnetite formation according to 359 the following equations:

$$360 Fe(CH_3COO)_3 + 3H_2O \rightarrow Fe(OH)_3 + 3CH_3COOH (5)$$

$$361 Fe(OH)_3 \to Fe_2O_3 + Fe_3O_4 (6)$$

At the 200 °C dwell temperature, elimination of acetate occurs through the direct thermal decomposition of iron acetate salts, according to ⁷⁸:

$$12 \text{ Fe}(CH_3COO)_3 = 4 \text{ Fe}_3O_4 + 18 \text{ CH}_3COCH_3 + 18 \text{ CO}_2 + O_2$$

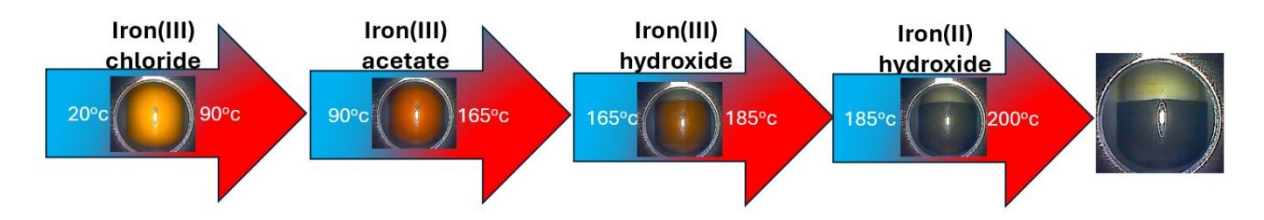


Fig 2 Image of reaction mixture during microwave synthesis demonstrating the different states present depending on reaction temperature transition. The time lapse in any temperature range depending on ramp rate will impact the nature and predominance of the species present.

We propose that the time taken to reach the microwave dwell temperature of 200 °C influences the composition of the reaction mixture and importantly that levels of acetate present influences final particle and aggregate sizes. The acetate is acting as a weak buffer to produce hydroxide ions *in situ* supporting the production of [Fe(OH)₃] and resulting in iron oxide precipitation and subsequent aggregation. Therefore, by altering the ramp time we control the degree of FeOAc conversion to Fe(OH)₃ in the early stages of MNP production which in turn controls the size of the initial particles produced. At a fast (2 minute) temperature ramp (ie 90 °C/min) to the dwell temperature, there is less iron hydroxide produced during the ramping period. At a slow (10 minute) temperature ramp (ie 18 °C/min) to the dwell temperature, there is more time for iron acetate to be converted to iron hydroxide during the ramping period, resulting in more maghemite and magnetite production during the ramping phase. Slowing down the time at which acetate decomposition takes place leads to further precipitation and aggregation, and controlled production of larger magnetic nanoparticles.

Fig 3 shows the FTIR spectrum obtained for MNP@CHO. The absorption at 520 cm⁻¹ is attributed to the octahedral Fe-O vibrational stretching of the iron-oxygen bond The slight non symmetry of this peak suggest that most of the iron present is in the form of magnetite and only a small amount of maghemite⁸³. The peak at 1724 cm⁻¹ corresponds to the C=O stretching vibration of the carbonyl bond. The peak at 2820 cm⁻¹ is associated with the asymmetric stretching of C-H bonds. These peaks indicate the presence of a magnetic core surrounded by aldehyde groups, as synthesised via the one-pot microwave method described.

Our IR analysis (Fig. 3) does not indicate a covalent link between Fe and aldehyde of the stability of glutaraldehyde to polymerise when aged or heated 79,80, we believe we are achieving coating of growing superparamagnetic iron oxide crystal structures with glutaraldehyde oligomers which still retain aldehyde groups. We believe the glutaraldehyde polymer chains become entrapped as the nanoparticle is forming allowing the glutaraldehyde groups to cover the MNP in a core-shell fashion. We do not fully understand the mechanism of agglomeration (clustering) but propose that it is associated with the glutaraldehyde oligomerising (growing in chain length) and partly acting as a binding agent (glue) between individual growing particles. Our assertion is in line with work by others who have shown that structures and assemblies of single cores can be stabilised into clusters of multi-core magnetic systems in the presence of hydrophilic and polymeric molecules 81,82 such as heparin and carbohydrates like dextran.

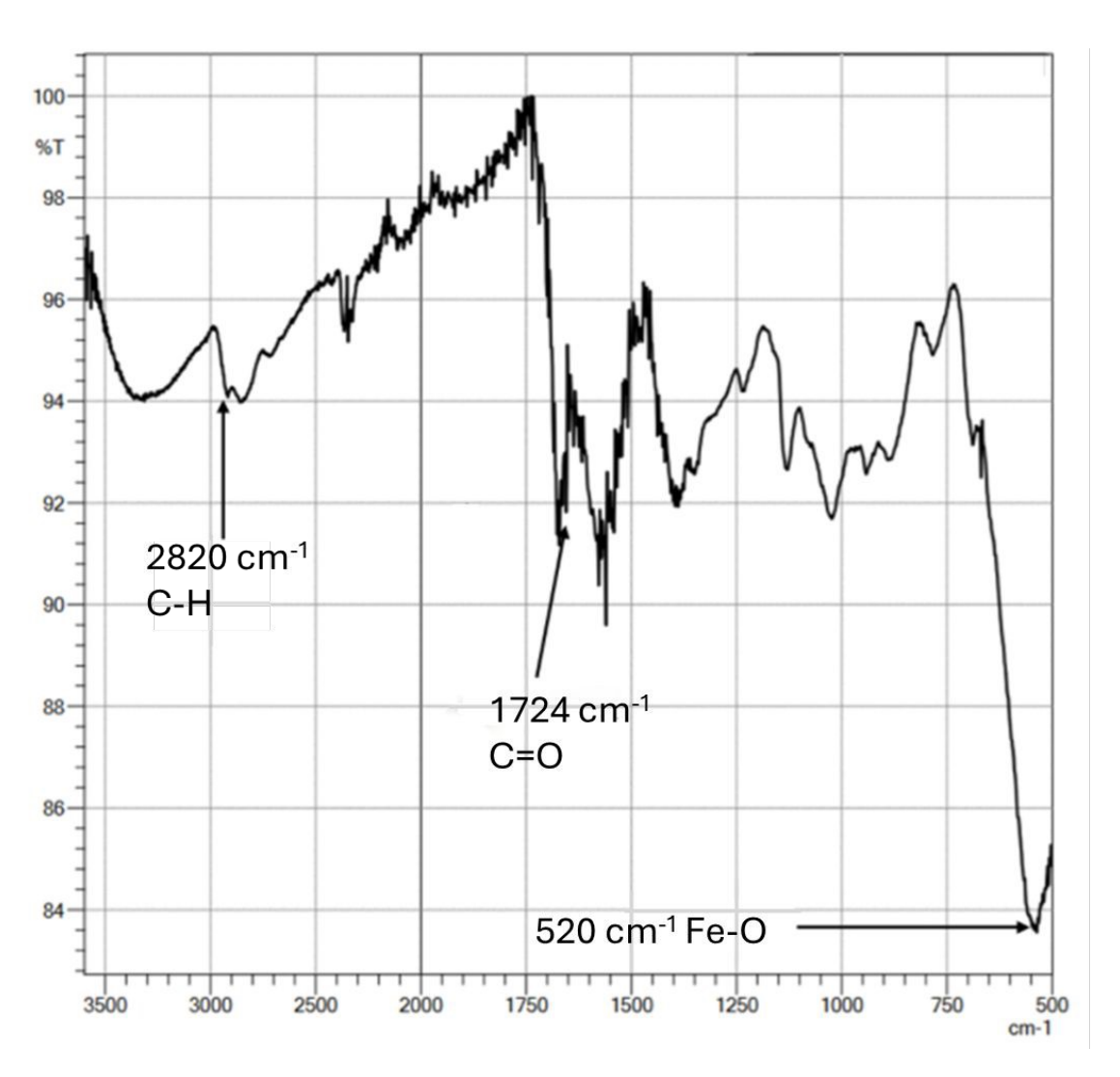


Fig 3: Infrared spectrum of MNP@CHO produced at 10 min ramp time followed by 20 min dwell time. The particles were oven dried at 110°C over 2 days prior to measurement at room temperature.

X-ray diffraction patterns are shown in Supplementary Fig. S2. All samples is controlled predominately Fe $_3$ O $_4$ (space group $Fd\overline{3}m$, a=8.400 Å) with s α -Fe $_2$ O $_3$ (space group $R\overline{3}cH$, a=5.0324 Å and c=13.7643 Å), both appearing as broad peaks in the diffraction patterns. Sharp peaks arrithmatable to NaCl (marked with *) are also present. The broad peak widths observed for the MNPs mean together with the close proximity of the expected peak positions of Fe $_3$ O $_4$ and α -Fe $_2$ O $_3$ results in some uncertainty in the exact ratios of Fe $_3$ O $_4$ and α -Fe $_2$ O $_3$. For example, the most instense MNP peak in the diffraction patterns was observed at 35.5° 2-theta and the (1 3 1) peak of Fe $_3$ O $_4$ is located at 35.4°, while the (1 -2 0) peak of α -Fe $_2$ O $_3$ occurs at 35.7°. Any variation in the amount of α -Fe $_2$ O $_3$ will cause asymmetry in the peaks and will cause uncertainty in the Scherrer calculation.

The particles after oven drying were imaged using transmission electron microscopy. Figures 4(a-d) show TEM images of MNP@CHO particles produced at 2-, 6-, 8- and 10-min ramp times respectively. Increasing the ramp time between 2-minutes (Fig. 4a) and 10-minutes (Fig. 4d) results in a corresponding increase in MNP@CHO core particle size between 7 ± 2 nm and 12.6 ± 3.2 nm respectively and cluster size of 91 ± 15 nm at 10 min (Fig. 4e). We could not identify any clustering at 2 min ramp time.

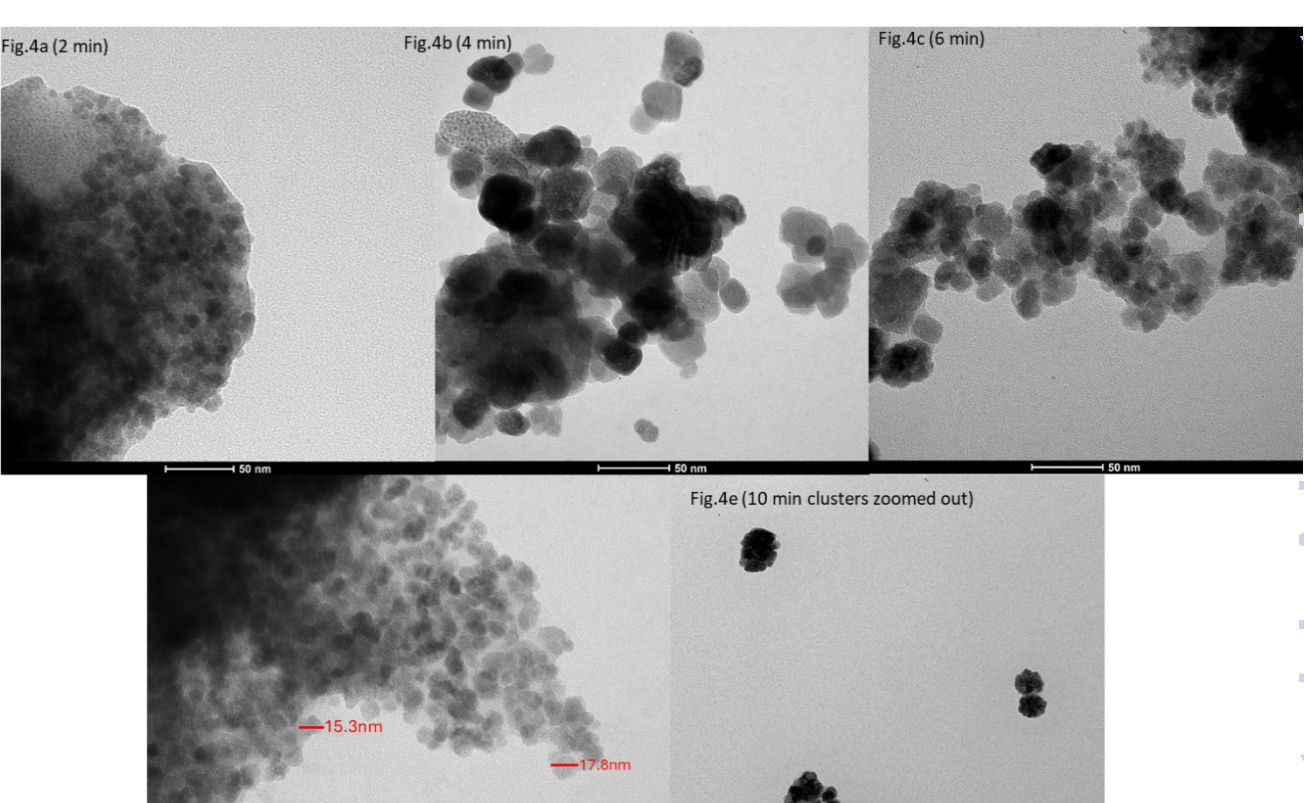


Fig 4. TEM of magnetic nanoparticles produced at a ramp period of (a) 2 min (90 °C/min), (b) 6 min (30 °C/min), (c) 8 min (22.5 °C/min) and (d) 10 min (12 °C/min). Fig 4(e) shows 10 min particles clustering at lower magnification. The particles increase in cluster size with increasing ramp time. Fig.4d average Particle size for individual magnetic nanoparticles was calculated to be 12.7nm \pm 3.7nm (Data represents mean \pm S.E.M., n = 100)

Fig.4d (10 min)

434

435

The TEM sizing of MNP@CHO formulations is on average smaller than the corresponding DLS sizes. Whereas DLS sizing is conducted in aquo and therefore represent a hydrodynamic diameter, the TEM measurements are conducted in vacuo and in a dried state. This has also been observed by Dingchen-Wen et al 84 in their study of chemical synthesis of MNPs.

436

437

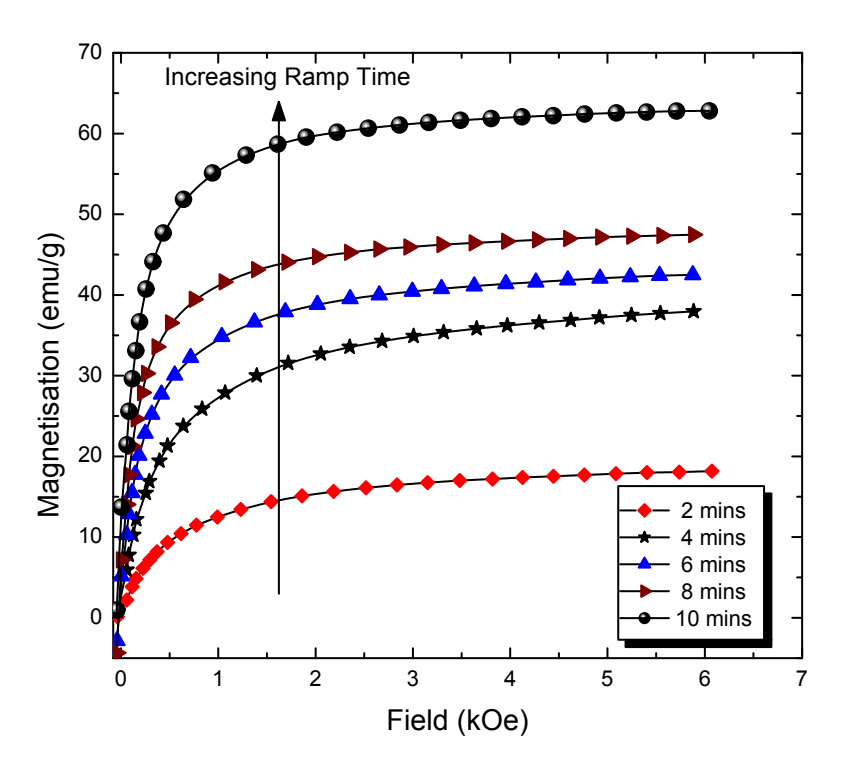
438

439

440 441

3.3 Magnetic Measurements and Sizing of MNP@CHO

Magnetisation curves as a function of applied field are shown in Fig. 5 from the series of samples with microwave ramp times in the range 2 to 10 mins. Only the first quadrants of the full M-H loops are shown for clarity, with the near closed curves of the loops having negligible coercivity and remanence that is indicative of the superparamagnetic state.



442

443

444

445 446

447

448

449 450

451

452

Fig. 5: Magnetisation curves of samples with increasing microwave ramp time. The increasing mass saturation magnetisation is consistent with increasing particle size as expected with magnetite particles on the nanoscale. The full loops are near-closed and therefore have very small coercivity and remanence, as shown for the sample with the highest values in the inset.

It is well known (e.g. 85) that the saturation magnetisation, M_s , for magnetite decreases from the bulk value of 92 emu/g, when in a multi-domain ferrimagnetic state, to lower values as a function of decreasing particle size when in the single-domain superparamagnetic state of size-order tens of nm. It is widely accepted that there are effectively 'magnetically dead' layers at, or near, the particle surface 86, leaving only the core that is magnetically responsive and thereby diluting the magnetic content within the volume (or mass) of the particle and

subsequent reduction in M_s values. In the bare particle case this is assigned to suffice online oxidisation and/or crystallographic disorder. Further dilution occurs when the nanoparticles are coated with surfactants, lipids and other functional agents, such as the Aldehyde of the magnetic measurements. As surface effects become more dominant with decreasing particle size, and subsequent increasing surface area, the reduction in M_s observed here is also consistent with decreasing particle size because of decreasing ramp time.

The indicative results of Fig. 5 were investigated further by using the magnetic sizing method of Chantrell⁸⁷. Briefly, the median particle diameter, D_m , and standard deviation, σ , of a lognormal distribution of particle sizes are calculated using

$$D_m = \left[\frac{18kT}{\pi M_b} \cdot \sqrt{\frac{\chi_i}{3\epsilon M_b} \cdot \frac{1}{H_0}} \right]^{1/3} \tag{7}$$

464 and

$$\sigma = \frac{1}{3} \left[\ln \left(\frac{3\chi_i}{\epsilon M_b \cdot 1/H_0} \right) \right]^{1/2} \tag{8}$$

where χ_i is the initial susceptibility, M_b the saturation magnetisation of the bulk material, ϵ the particle volume fraction, k is the Boltzmann constant and T the absolute temperature. The Langevin function provides a good theoretical description of superparamagnetic curves and is used in the Chantrell method to derive (7) and (8). At large fields, H, it reduces to a linear expression such that a plot of M as a function of 1/H will result in a linear fit that crosses the abscissa when M = zero at the point $1/H_0$. Experimental measurements of χ_i , $1/H_0$ and ϵM_b may then be used to determine D_m and σ using equations (7) and (8).

The outcome is shown in Fig. 6 which shows a clear trend of an overall increase in particle size with increasing ramp time as was found in the in the DLS and TEM results. It confirms the increasing saturation magnetisation is a result of increasing particle size due to increasing ramp times as can be seen in the inset of Fig. 6, where the M_s values are those extrapolated from the data of Fig. 5 using M verses 1/H at high applied fields, to the crossing point of the ordinate i.e. when the applied field is tending to infinity.

There is no obvious trend in the values of σ shown on the right-hand axis of Fig. 6. The largest value of 0.33 is associated with the 4-minute sample and suggests this has the widest range of particle size distribution. Careful observation of the same sample's magnetisation curve in Fig. 5 also shows this is further away from saturation than the other samples, with a steeper gradient on the approach to 6 kOe. The assumption inherent in the sizing method is of a lognormal distribution and any deviation from this along with its largest σ value may explain, in part at least, the noticeable difference in the magnetisation curve towards the maximum applied field.

489

490

491

492

493 494

495

496

497 498

499

500 501

502503

504

505

506

507

508 509

510

511

512

Table 1 compares median particle size determined using magnetic measurements which magnetic measurements which makes the magnetic measurements with the magnetic measurements with the magnetic measurements and the magnetic measurements are made in the magnetic measurements. agglomerate size results determined using TEM and DLS at selected ramp times. The magnetic core size measurement and calculations refer to the size of individual magnetic cores ie single particle core size, not agglomerates. The TEM images taken are suggesting we can get clustering or agglomeration with increasing ramp time. It was difficult to discern individual particles at all ramp times using TEM but where we could for example at 10 min ramp time (Fig. 4d), the average individual particle size determined by TEM (12.6 nm ±3.2 nm) is in good agreement with magnetic core size determination of 11.25 nm. As TEM measurements include all the particles, including the magnetically dead outer layers, they are expected to be larger than those of the magnetic measurements. DLS gives the hydrodynamic diameter of particles in an aqueous suspension. We believe the DLS size is the summation of the MNP magnetic core size plus a glutaraldehyde shell layer plus some agglomeration of the MNPs. Therefore, whereas all methods of measurement used show a correlation with ramp time, the size increases in the order: Mag core < TEM < DLS. Crystallite size was determined from XRD measurements using the Scherrer calculation using 2 and 10 min MNP@CHO particles giving crystallite sizes of 7.7 nm and 9.3 nm respectively. Whereas the 2 min particles are in good agreement with magnetic and TEM sizing, there is some significant deviation in the 10 min crystallite size calculation.

Our results demonstrate a correlation (across measurement techniques) between increase in particle/agglomerate size and increasing ramp time.

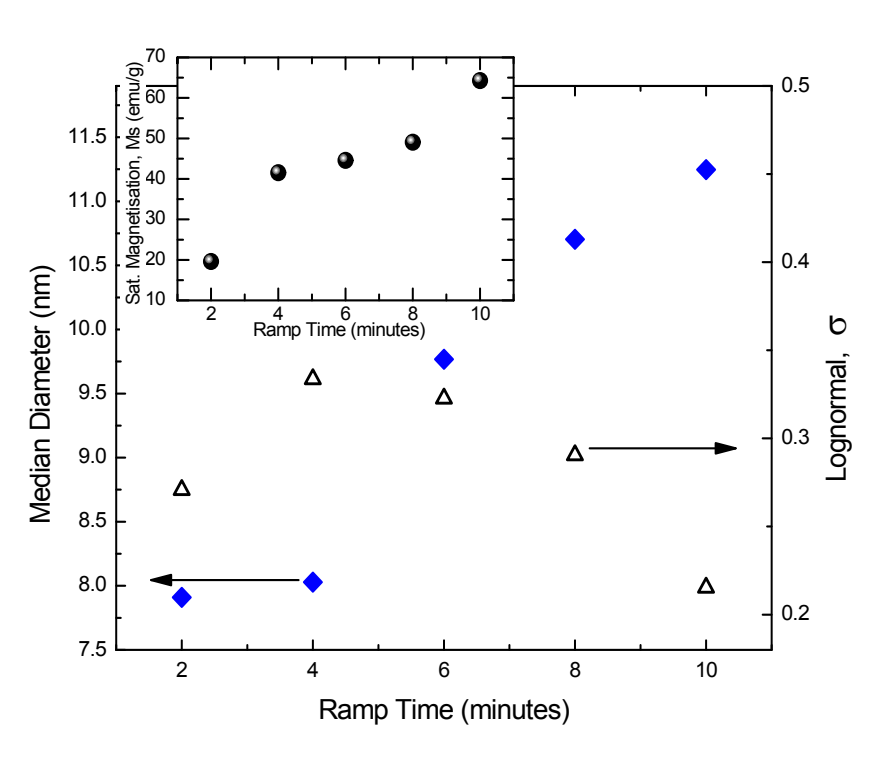


Fig. 6: Median particle diameter and lognormal σ values as functions of ramp time following the method of Chantrell ⁸⁷. The decreasing particle size with decreasing ramp time confirms this is the cause of the drop in saturation magnetisation of the inset obtained by extrapolation of the data from Fig. 5. There is no overall trend in the σ values that indicate the 4-minute sample has the widest range of particle sizes in its distribution and the 10-minute sample the narrowest.

Table 1 Comparison of measurement techniques for the sizing of MNP particles and or New Article Online agglomerates. All methods confirm that there is an increase in entity size with increase in ramp time.

Ramp time	Magnetic core size		TEM size clusters	DLS size
(min)	D _{median} (nm)	σ	(nm)	(nm)
2	7.91	0.27	8.5 ± 2	14.9 ± 8
6	9.77	0.32	23 ± 6	60 ± 7
10	11.25	0.22	91 ± 15	122 ± 49

3.4 Impact of MNP Size on Solid Phase Synthesis of Smart Polymers

Recently there has been growing interest in the synthesis of polymers with biorecognition capability and their application in diagnostics, biological extraction and therapeutics. Molecularly imprinted polymers are a class of artificial receptor. They can be synthetically grown around a target biological ^{46, 75, 88, 89} resulting in the imparting of complementary recognition sites within the crosslinked polymer. We recently reported that MNPs modified with a protein can be used as a solid substrate to facilitate the manufacture of nanoscale MIPs²³. Subsequently, we showed that the nanoMIPs could be harvested and the MNP@protein could be recycled and re-used to scale up the yield of nanoMIPs. Here we show that the MNP size is critical to the effective functioning of the material for solid phase synthesis of nanoMIPs (See Fig. 7 for a schematic of the process).

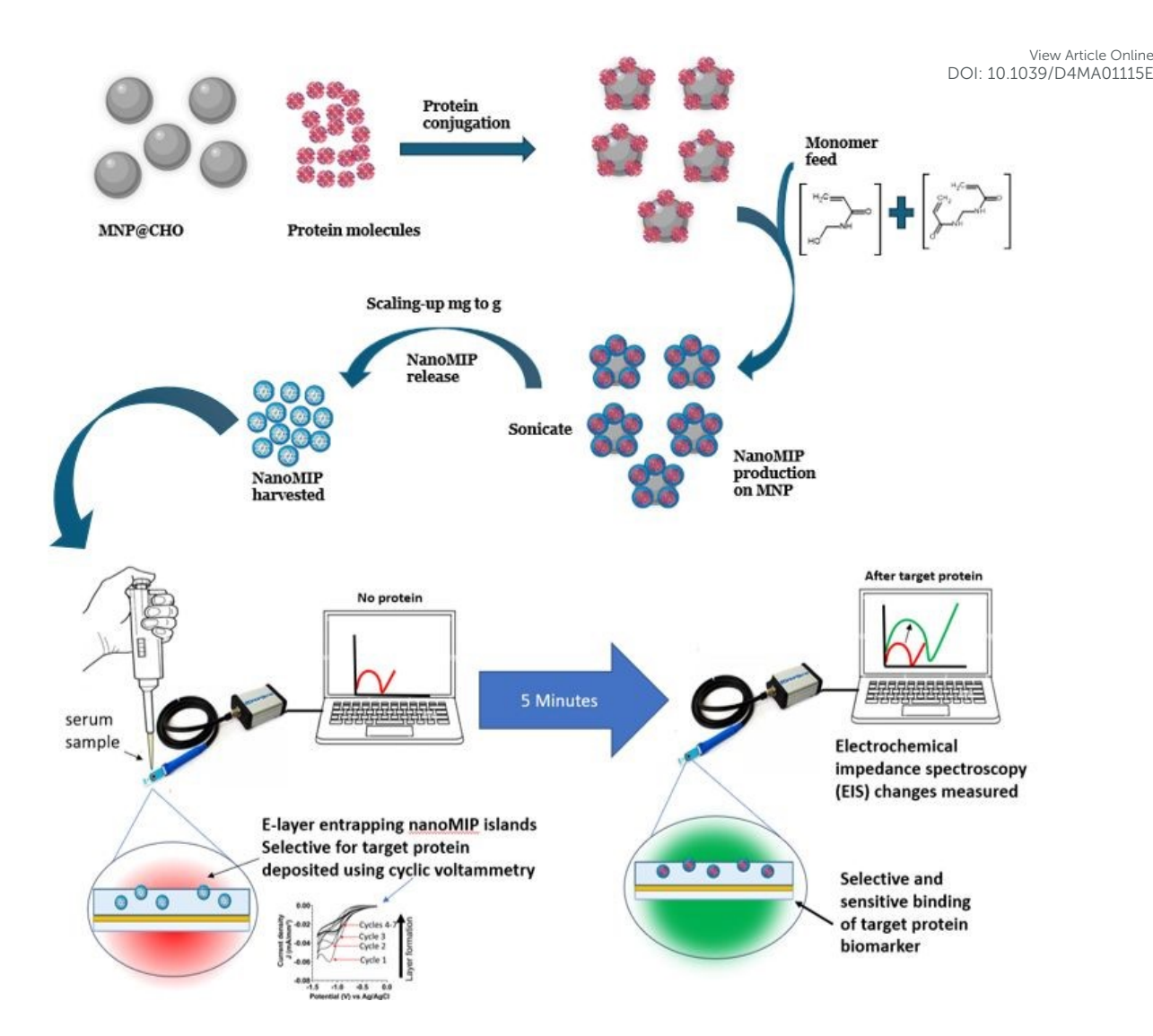


Fig 7: Schematic of nanoMIP polymer synthesis on MNP solid phase. The MNP@CHO is first conjugated with target protein to give MNP@protein. In the presence of monomer and crosslinker feed, the nanoMIPs grow specifically around the MNP@protein. Once released and harvested, the nanoMIP is integrated to a disposable screen-printed electrode for biosensor determination of protein biomarker.

We used mass equivalents of as produced MNP@CHO particles at 2-10 min ramp times in the synthesis of nanoMIPs. The MNP@CHO were first conjugated with bovine haemoglobin (BHb) as target (template). The resulting MNP@CHO@BHb particles were then used as the solid phase to produce nanoMIPs selective for BHb. The nanoMIPs produced were subsequently released from the MNP and then size characterised using DLS. The isolated nanoMIPs were integrated to a disposable screen-printed gold electrode for electrochemical determination of protein and non-target protein rebinding from test solutions. Electrochemical impedance spectroscopy (EIS) was used to interrogate and quantify protein binding. EIS is a suitable sensitive technique to measure nanomolar to picomolar levels of target binding to the synthetic receptor ⁹⁰. It relies on interrogating the electrochemical properties of the nanoMIP/electrode interface in the presence of a suitable redox marker

549

550

551

552

553

554555

556

557558

559

560

561

562563

564

565

566

(ferrocyanide was used here) at a standard potential of 0.1 V (± 0.01 V) at multiple View Article Online (ferrocyanide was used here) at a standard potential of 0.1 V (± 0.01 V) at multiple View Article Online (ferrocyanide was used here) at a standard potential of 0.1 V (± 0.01 V) at multiple (Fig. 10.1039/D4MA01115E) at a standard potential of 0.1 V (± 0.01 V) at multiple (Fig. 10.1039/D4MA01115E) at a standard potential of 0.1 V (± 0.01 V) at multiple (Fig. 10.1039/D4MA01115E) at a standard potential of 0.1 V (± 0.01 V) at multiple (Fig. 10.1039/D4MA01115E) at a standard potential of 0.1 V (± 0.01 V) at multiple (Fig. 10.1039/D4MA01115E) at a standard potential of 0.1 V (± 0.01 V) at multiple (Fig. 10.1039/D4MA01115E) at a standard potential of 0.1 V (± 0.01 V) at multiple (Fig. 10.1039/D4MA01115E) at a standard potential of 0.1 V (± 0.01 V) at multiple (Fig. 10.1039/D4MA01115E) at a standard potential of 0.1 V (± 0.01 V) at multiple (Fig. 10.1039/D4MA01115E) at a standard potential of 0.1 V (± 0.01 V) at multiple (Fig. 10.1039/D4MA01115E) at a standard potential of 0.1 V (± 0.01 V) at multiple (Fig. 10.1039/D4MA01115E) at a standard potential of 0.1 V (± 0.01 V) at multiple (Fig. 10.1039/D4MA01115E) at a standard potential of 0.1 V (± 0.01 V) at multiple (Fig. 10.1039/D4MA01115E) at a standard potential of 0.1 V (± 0.01 V) at multiple (Fig. 10.1039/D4MA01115E) at a standard potential of 0.1 V (± 0.01 V) at multiple (Fig. 10.1039/D4MA01115E) at a standard potential of 0.1 V (± 0.01 V) at multiple (Fig. 10.1039/D4MA01115E) at a standard potential of 0.1 V (± 0.01 V) at multiple (Fig. 10.1039/D4MA01115E) at a standard potential of 0.1 V (± 0.01 V) at multiple (Fig. 10.1039/D4MA01115E) at a standard potential of 0.1 V (± 0.01 V) at multiple (Fig. 10.1039/D4MA01115E) at a standard potential of 0.1 V (± 0.01 V) at multiple (Fig. 10.1039/D4MA01115E) at a standard potential of 0.1 V (± 0.01 V) at multiple (Fig. 10.1039/D4MA01115E) at a standard potential of 0.1 V (± 0.01 V) at multiple (Fig. 10.1039/D4MA01115E) at frequencies, and a sinusoidal potential peak-to-peak with amplitude 0.01 V in the 0.1 -100000 Hz frequency range. The interface is modelled on the Randles circuit. We measured the change in charge transfer resistance (ΔR_{CT}) when electrode was modified with nanoMIP which was a function of resistance of ferrocyanide redox marker diffusion to the working electrode²³. When target protein was subsequently added, it selectively bound to the nanoMIP at the nanoMIP/electrode interface creating an additional barrier to ferrocyanide redox marker diffusion. There is a corresponding increase in ΔR_{CT} with increase in target protein binding. Figs S1-S5 compare plots of [BHb] versus ΔR_{CT} for nanoMIPs synthesised on BHb functionalised MNP@CHO magnetic nanoparticles produced at ramp times of 2 min (Fig S3), 4 min (Fig S4), 6 min (Fig. S5), 8 min (Fig. S6) and 10 min (Fig. S7). Table 2 summarises the impact of MNP size (measured using DLS) on subsequent nanoMIP synthesis parameters including nanoMIP particle size, yield and affinity factors such as the equilibrium dissociation constant (K_D) and the relative response of the biosensor to target protein (BHb) and non-target protein (bovine serum albumin; BSA). The equilibrium dissociation constant K_D for each nanoMIP batch was determined using the Hill-Langmuir method using data from Figures S2-S6.

Table 2 Impact of MNP size on subsequent nanoMIP particle size, yield and affinity factors. Data represents mean \pm S.E.M., n = 3 and selectivity factor was determined using the ratio of ΔR_{CT} of target (BHb) bound to MIP and ΔR_{CT} of non-target (BSA) bound to MIP.

Microwave Ramp time (min)	DLS size of MNP@CHO (nm)	DLS size of nanoMIP (nm)	Yield of NanoMIP (mg/mL)	K _D (mol L ⁻¹)	Selectivity Factor (Target : non target signal ratio @1 nM)
2	14±8	80±14	0.13±0.06	1.40 x 10 ⁻¹⁰ ±2.79 x 10 ⁻¹²	49:1
4	46±12	123±41	1.6±0.3	2.01 x 10 ⁻¹¹ ± 5.05 x 10 ⁻¹²	75:1
6	60±7	119±51	3.7±0.3	1.75 x 10 ⁻¹¹ ± 2.61 x 10 ⁻¹²	166 : 1
8	84±11	120±57	6.5±0.3	2.40 x10 ⁻¹¹ ± 9.21 x 10 ⁻¹²	100:1
10	122±49	125±43	12.3±2.5	3.47 x 10 ⁻¹¹ ± 2.35 x10 ⁻¹²	188:1

567

568

569 570

571

572

573

574575

576

While a low K_D of between 10⁻⁹ to 10⁻¹¹ mol L⁻¹ gives an indication of tendency of the nanoMIP to tightly bind with the target with affinities akin to a monoclonal antibody, the selectivity factor is an effective measure of how more effective the MIP is at picking out its target protein (complement) compared with a non-target (non-complementary) protein. We demonstrate a direct correlation between MNP@CHO size (and subsequently MNP@protein size) with nanoMIP yield. While all particles resulted in the production of nanoMIPs with high affinity, nanoMIP selectivity, nanoMIP yield increased with increasing ramp time with 10 min ramp time returning the best yield of nanoMIPs. The least effective nanoMIPs were produced using the 2 min ramp time particles. Interestingly, the DLS size of

nanoMIP is approximately 120 nm and independent of ramp time between 4 and No.109 10.1039/D4MA01115E
 minutes. We did not study the 15 min ramp time particles as their clumping sludge-like
 characteristics did not make them ideal candidates for nanoMIP manufacture.

We demonstrate a simple, economical, rapid and scalable microwave method to produce magnetite-based magnetic nanoparticles (MNPs) at a desired size and their application to facile synthesis of high value polymer products such as nanoMIPs. Our size-tuned MNPs have many potential applications in biological extraction (when conjugated with antibodies or nanoMIPs) which we are currently investigating as well as applications in medical imaging and therapeutics.

Conclusions

Aldehyde functionalised magnetic nanoparticles (MNP@CHO) of tuneable size can be produced within 20-30 minutes. The initial temperature ramp used prior to the 20 min dwell time for the MNP synthesis is crucial to influencing both the MNP particle and clustering size as determined using transmission electron microscopy. We present a mechanism based on rate of acetate decomposition during MNP particle and cluster formation. Altering the ramp time between 2- and 10-min results in a corresponding increase in MNP@CHO particle sizes between 7 nm and 91 nm measured using TEM and cluster (stable agglomerate) sizes of between 36 nm and 122 nm measured using DLS.

We also demonstrate their application to the development of nanoscale molecularly imprinted polymer (NanoMIP) receptor-based electrochemical sensors. We demonstrate that there is an optimal MNP size for highly efficient MNP-based nanoMIP production which is key to mass production and commercialisation of low-cost and sustainable bespoke size-tuned MNPs and antibody replacement technologies.

Data Availability

All data are available within the article and its Supplementary Information files and from the authors upon request.

Acknowledgments

The authors are grateful to the University of Central Lancashire, the Royal Society of Chemistry COVID-19 Action fund (H20-188), the Daiwa Anglo-Japanese Foundation (13094/13916) and The Royal Society (IES\R3\193093) for funding this work. We wish to thank Dr Jennifer Simpson (The Pirbright Institute) for the providing the service in obtaining transmission electron microscope images of the MNPs.

619

620

621

622

623

624

625

View Article Online DOI: 10.1039/D4MA01115E

s Article. Published on 11 February 2025. Downloaded on 2/14/2025 1:59:45 PM.	This article is licensed under a Creative Commons Attribution 3.0 Unported Licence.
Open Acces	cc)) BY

614	SMR conceived, designed and directed the study and wrote the manuscript. ANS and WJS
615	prepared the MNPs. ANS performed nanoMIP synthesis, DLS and TEM characterization and
616	electrochemical studies. JER performed XRD. TM performed magnetic measurements and
617	data analysis. SMR, ANS, JER and TM performed the analysis. All authors contributed to
618	manuscript revision, read, and approved the submitted version.

Competing Interests

Author Contribution

The authors declare that the research was conducted in the absence of any commercial or financial relationships that could be construed as a potential conflict of interest.

21

View Article Online

DOI: 10.1039/D4MA01115E

This article is licensed under a Creative Commons Attribution 3.0 Unported Licence.

645

Open Access Article. Published on 11 February 2025. Downloaded on 2/14/2025 1:59:45 PM.

- H. M. Williams, Bioscience Horizons: The International Journal of Student Research, 2017, 10. 627 1.
- 628 2. D. A. Alromi, S. Y. Madani and A. Seifalian, Polymers (Basel), 2021, 13.
- A. Akbarzadeh, M. Samiei and S. Davaran, Nanoscale Res Lett, 2012, 7, 144. 629 3.
- 630 4. H. Markides, M. Rotherham and A. J. El Haj, Journal of Nanomaterials, 2012, 2012, 614094.
- N. Malhotra, J. S. Lee, R. A. D. Liman, J. M. S. Ruallo, O. B. Villaflores, T. R. Ger and C. D. 631 5. 632 Hsiao, Molecules, 2020, 25.
- 633 Y. Chen and S. Hou, Cell Death Discovery, 2023, 9, 195. 6.
- 634 C. Das, N. N. Ghosh, V. Pulhani, G. Biswas and P. Singhal, RSC Advances, 2023, 13, 15015-7. 635 15023.
- 636 8. J. Dulińska-Litewka, A. Łazarczyk, P. Hałubiec, O. Szafrański, K. Karnas and A. Karewicz, 637 Materials (Basel), 2019, 12.
- 638 9. C. T. Yavuz, J. T. Mayo, W. W. Yu, A. Prakash, J. C. Falkner, S. Yean, L. Cong, H. J. Shipley, A. 639 Kan, M. Tomson, D. Natelson and V. L. Colvin, Science, 2006, 314, 964-967.
- 640 Y. W. Jun, Y. M. Huh, J. S. Choi, J. H. Lee, H. T. Song, S. Kim, S. Yoon, K. S. Kim, J. S. Shin, J. S. 10. 641 Suh and J. Cheon, J Am Chem Soc, 2005, 127, 5732-5733.
- 642 11. N. Lamichhane, M. E. Sharifabad, B. Hodgson, T. Mercer and T. Sen, in Nanoparticle Therapeutics, eds. P. Kesharwani and K. K. Singh, Academic Press, 2022, DOI: 643 644 https://doi.org/10.1016/B978-0-12-820757-4.00003-X, pp. 455-497.
 - 12. D. J. Dunlop, Journal of Geophysical Research (1896-1977), 1973, 78, 1780-1793.
- 646 13. M. Z. Iqbal, G. I. Dar, I. Ali and A. Wu, in Nanomedicine in Brain Diseases: Principles and 647 Application, ed. X. Xue, Springer Singapore, Singapore, 2019, DOI: 10.1007/978-981-13-648 8731-9_10, pp. 269-313.
- 649 14. Z. R. Stephen, F. M. Kievit and M. Zhang, Mater Today (Kidlington), 2011, 14, 330-338.
- 650 T. Tegafaw, S. Liu, M. Y. Ahmad, A. Saidi, D. Zhao, Y. Liu, S. W. Nam, Y. Chang and G. H. Lee, 15. 651 Pharmaceutics, 2023, 15.
- 652 16. Y. Patil-Sen, E. Torino, F. De Sarno, A. M. Ponsiglione, V. Chhabria, W. Ahmed and T. Mercer, 653 Nanotechnology, 2020, **31**, 375102.
- 654 17. M. Wierucka and M. Biziuk, TrAC Trends in Analytical Chemistry, 2014, 59, 50-58.
- 655 M. Khajeh and A. Khajeh, International Journal of Green Nanotechnology: Physics and 18. 656 Chemistry, 2009, 1, P51-P56.
- 657 A. J. Giustini, A. A. Petryk, S. M. Cassim, J. A. Tate, I. Baker and P. J. Hoopes, Nano Life, 2010, 19. 658 1.
- 659 20. X. Liu, Y. Zhang, Y. Wang, W. Zhu, G. Li, X. Ma, Y. Zhang, S. Chen, S. Tiwari, K. Shi, S. Zhang, H. 660 M. Fan, Y. X. Zhao and X. J. Liang, *Theranostics*, 2020, **10**, 3793-3815.
- 661 21. L. Lartigue, P. Hugounenq, D. Alloyeau, S. P. Clarke, M. Lévy, J.-C. Bacri, R. Bazzi, D. F. 662 Brougham, C. Wilhelm and F. Gazeau, ACS Nano, 2012, 6, 10935-10949.
- S. Dutz, M. Kettering, I. Hilger, R. Müller and M. Zeisberger, Nanotechnology, 2011, 22, 663 22. 664 265102.
- 665 23. S. M. Reddy, A. N. Stephen, M. A. Holden, W. J. Stockburn and S. R. Dennison, Biomaterials 666 Science, 2024, DOI: 10.1039/D4BM00990H.
- 667 24. D. Hu, Y. Wang and Q. Song, *Particuology*, 2009, **7**, 363-367.
- Y. Mizukoshi, T. Shuto, N. Masahashi and S. Tanabe, Ultrasonics Sonochemistry, 2009, 16, 668 25. 669 525-531.
- 670 I. Nedkov, T. Merodiiska, L. Slavov, R. E. Vandenberghe, Y. Kusano and J. Takada, Journal of 26. 671 Magnetism and Magnetic Materials, 2006, 300, 358-367.
- 672 27. H. Pardoe, W. Chua-anusorn, T. G. St. Pierre and J. Dobson, Journal of Magnetism and 673 Magnetic Materials, 2001, 225, 41-46.
- S. Fakurpur Shirejini, S. M. Dehnavi and M. Jahanfar, Chemical Engineering Research and 674 28. 675 Design, 2023, 190, 580-589.
- 676 29. J. Liu, L. Wang, J. Wang and L. Zhang, Materials Research Bulletin, 2013, 48, 416-421.

- 677 30. Y. Chen, J.-G. Zhang, Z. Wang and Z. Zhou, *Applied Sciences*, 2019, **9**, 5157. View Article Online DOI: 10.1039/D4MA01115E
- 31. Z. Huang, K. Wu, Q.-H. Yu, Y.-Y. Wang, J. Xing and T.-L. Xia, *Chemical Physics Letters*, 2016,
 664, 219-225.
- 32. X. Yang, W. Jiang, L. Liu, B. Chen, S. Wu, D. Sun and F. Li, *Journal of Magnetism and Magnetic Materials*, 2012, **324**, 2249-2257.
- 682 33. M. Tadic, M. Panjan, V. Damnjanovic and I. Milosevic, *Applied Surface Science*, 2014, **320**, 183-187.
- 684 34. N. A. Yazid and Y. C. Joon, AIP Conference Proceedings, 2019, 2124.
- H. Köçkar and O. Karaagac, *Journal of Materials Science: Materials in Electronics*, 2021, **32**, 13673-13684.
- 687 36. O. u. Rahman, S. C. Mohapatra and S. Ahmad, *Materials Chemistry and Physics*, 2012, **132**, 688 196-202.
- 689 37. K. Petcharoen and A. Sirivat, Materials Science and Engineering: B, 2012, 177, 421-427.
- 590 38. D. Lokhat, S. Brijlal, D. E. Naidoo, C. Premraj and E. Kadwa, *Industrial & amp; Engineering Chemistry Research*, 2022.
- 692 39. M. Jafari Eskandari and I. Hasanzadeh, *Materials Science and Engineering: B*, 2021, **266**, 693 115050.
- 40. M. Zahid, N. Nadeem, M. A. Hanif, I. A. Bhatti, H. N. Bhatti and G. Mustafa, in *Magnetic* 695 *Nanostructures : Environmental and Agricultural Applications*, eds. K. A. Abd-Elsalam, M. A.
 696 Mohamed and R. Prasad, Springer International Publishing, Cham, 2019, DOI: 10.1007/978 697 3-030-16439-3 10, pp. 181-212.
- 698 41. G. F. Stiufiuc and R. I. Stiufiuc, *Applied Sciences*, 2024, **14**, 1623.
- 42. A. Ali, H. Zafar, M. Zia, I. Ul Haq, A. R. Phull, J. S. Ali and A. Hussain, *Nanotechnol Sci Appl*,
 2016, 9, 49-67.
- 701 43. N. Mizutani, T. Iwasaki, S. Watano, T. Yanagida and T. Kawai, *Current Applied Physics*, 2010, 702 **10**, 801-806.
- 703 44. E. Aivazoglou, E. Metaxa and E. Hristoforou, AIP Advances, 2017, 8.
- 704 45. L. M. Kustov, E. M. Kostyukhin, E. Y. Korneeva and A. L. Kustov, *Russian Chemical Bulletin*, 2023, **72**, 583-601.
- 706 46. M. Sullivan, W. Stockburn, P. Hawes, T. Mercer and S. Reddy, *Nanotechnology*, 2020, 32,
 707 095502.
- 708 47. Z. Klencsár, A. Ábrahám, L. Szabó, E. G. Szabó, S. Stichleutner, E. Kuzmann, Z. Homonnay and
 709 G. Tolnai, *Materials Chemistry and Physics*, 2019, 223, 122-132.
- 48. L. M. Cursaru, R. M. Piticescu, D. V. Dragut, R. Morel, C. Thébault, M. Carrière, H. Joisten and
 B. Dieny, *Nanomaterials*, 2020, 10, 1500.
- 712 49. H. Al-Madhagi, V. Yazbik, W. Abdelwahed and L. Alchab, *BioNanoScience*, 2023, **13**, 853-859.
- 713 50. M. S. Islam, Y. Kusumoto, J. Kurawaki, M. D. Abdulla-Al-Mamun and H. Manaka, *Bulletin of Materials Science*, 2012, **35**, 1047-1053.
- 715 51. A. R. Trifoi, E. Matei, M. Râpă, A.-C. Berbecaru, C. Panaitescu, I. Banu and R. Doukeh, 716 *Reaction Kinetics, Mechanisms and Catalysis*, 2023, **136**, 2835-2874.
- 717 52. X. Wu, H. Choe, J. Strayer, J. Gómez-Pastora, M. Zborowski, B. Wyslouzil and J. Chalmers, 718 *Nanoscale*, 2024, **16**, 7041-7057.
- 719 53. A. J. Willis, S. P. Pernal, Z. A. Gaertner, S. S. Lakka, M. E. Sabo, F. M. Creighton and H. H. 720 Engelhard, *Int J Nanomedicine*, 2020, **15**, 4105-4123.
- 721 54. F. L. Durhuus, L. H. Wandall, M. H. Boisen, M. Kure, M. Beleggia and C. Frandsen, *Nanoscale*,
 722 2021, 13, 1970-1981.
- 723 55. Z. Cai, C. Wu, L. Yang, D. Wang and H. Ai, *ACS Biomaterials Science & Engineering*, 2020, 6,
 724 2533-2542.
- 725 56. S. Sharma, H. Sharma and R. Sharma, *Chemistry of Inorganic Materials*, 2024, **2**, 100035.
- 726 57. A. G. Kolhatkar, A. C. Jamison, D. Litvinov, R. C. Willson and T. R. Lee, *Int J Mol Sci*, 2013, **14**, 15977-16009.

Materials Advances Accepted Manuscript

- Y. Hadadian, H. Masoomi, A. Dinari, C. Ryu, S. Hwang, S. Kim, B. k. Cho, J. Y. Lee and J. Yoʻley Article Online On 728 58. 729 ACS Omega, 2022, 7, 15996-16012.
- L. Gloag, M. Mehdipour, D. Chen, R. D. Tilley and J. J. Gooding, Advanced Materials, 2019, 730 59. 731 **31**, 1904385.
- 732 60. L. C. Wu, Y. Zhang, G. Steinberg, H. Qu, S. Huang, M. Cheng, T. Bliss, F. Du, J. Rao, G. Song, L. 733 Pisani, T. Doyle, S. Conolly, K. Krishnan, G. Grant and M. Wintermark, American Journal of 734 Neuroradiology, 2019, 40, 206.
- 735 S. M. Dadfar, K. Roemhild, N. I. Drude, S. von Stillfried, R. Knüchel, F. Kiessling and T. 61. 736 Lammers, Advanced Drug Delivery Reviews, 2019, 138, 302-325.
- 737 62. J. Medinger, M. Nedyalkova and M. Lattuada, Nanomaterials (Basel), 2021, 11.
- 738 63. Y. Chen, J. Zhang, Z. Wang and Z. Zhou, Applied Sciences, 2019, 9, 5157.
- 739 F. Fiévet, S. Ammar-Merah, R. Brayner, F. Chau, M. Giraud, F. Mammeri, J. Peron, J. Y. 64. 740 Piquemal, L. Sicard and G. Viau, Chemical Society Reviews, 2018, 47, 5187-5233.
- 741 M. C. Mascolo, Y. Pei and T. A. Ring, *Materials (Basel)*, 2013, **6**, 5549-5567. 65.
- 742 66. L. Panariello, M. O. Besenhard, S. Damilos, A. Sergides, V. Sebastian, S. Irusta, J. Tang, N. T. K. 743 Thanh and A. Gavriilidis, Chemical Engineering and Processing - Process Intensification, 2022, 744 **182**, 109198.
- 745 67. M. O. Besenhard, L. Panariello, C. Kiefer, A. P. LaGrow, L. Storozhuk, F. Perton, S. Begin, D. 746 Mertz, N. T. K. Thanh and A. Gavriilidis, *Nanoscale*, 2021, **13**, 8795-8805.
- 747 M. O. Besenhard, A. P. LaGrow, A. Hodzic, M. Kriechbaum, L. Panariello, G. Bais, K. Loizou, S. 68. 748 Damilos, M. Margarida Cruz, N. T. K. Thanh and A. Gavriilidis, Chemical Engineering Journal, 749 2020, **399**, 125740.
- 750 69. F. Canfarotta, A. Poma, A. Guerreiro and S. Piletsky, Nature Protocols, 2016, 11, 443-455.
- T. Hix-Janssens, J. R. Davies, N. W. Turner, B. Sellergren and M. V. Sullivan, Analytical and 751 70. 752 Bioanalytical Chemistry, 2024, DOI: 10.1007/s00216-024-05395-6.
- 753 R. Mahajan, M. Rouhi, S. Shinde, T. Bedwell, A. Incel, L. Mavliutova, S. Piletsky, I. A. Nicholls 71. 754 and B. Sellergren, Angewandte Chemie International Edition, 2019, 58, 727-730.
- 755 72. S. Lyons, P. Baile Pomares, L. Vidal, K. McGarry, A. Morrin and D. F. Brougham, Langmuir, 756 2023, 39, 8100-8108.
- 757 73. C. Comanescu, Coatings, 2023, 13, 1772.
- 758 74. A. Aharoni, Journal of Applied Physics, 1998, 83, 3432-3434.
- 759 75. A. Stephen, S. Dennison, M. Holden and S. Reddy, *The Analyst*, 2023, **148**.
- 760 76. Z. Kozakova, I. Kuritka, N. E. Kazantseva, V. Babayan, M. Pastorek, M. Machovsky, P. Bazant 761 and P. Saha, Dalton Transactions, 2015, 44, 21099-21108.
- 762 77. W. Ma, P. M. Gehret, R. E. Hoff, L. P. Kelly and W. H. Suh, Journal, 2019, 9.
- A. Laurikėnas, J. Barkauskas, J. Reklaitis, G. Niaura, D. Baltrūnas and A. Kareiva, Lithuanian 763 78. 764 Journal of Physics, 2016, 56.
- K. E. Rasmussen and J. Albrechtsen, Histochemistry, 1974, 38, 19-26. 765 79.
- 766 80. I. Migneault, C. Dartiguenave, M. J. Bertrand and K. C. Waldron, BioTechniques, 2004, 37, 767 790-802.
- 768 81. D. Sarkar and P. Somasundaran, *Langmuir*, 2004, **20**, 4657-4664.
- 769 82. E. P. K. Currie, W. Norde and M. A. Cohen Stuart, Advances in Colloid and Interface Science, 770 2003, **100-102**, 205-265.
- M. Stoia, R. Istratie and C. Păcurariu, Journal of Thermal Analysis and Calorimetry, 2016, 125, 771 83. 772 1185-1198.
- 773 84. D. Wen, T. Ralph, J. Han, S. Bradley, M. J. Giansiracusa, V. Mitchell, C. Boskovic and N. 774 Kirkwood, The Journal of Physical Chemistry C, 2023, 127, 9164-9172.
- 775 M. C. Mascolo, Y. Pei and T. A. Ring, *Journal*, 2013, **6**, 5549-5567. 85.
- 776 86. K. O'Grady, G. V. Fernandez and A. Hirohata, Particulate and Granular Magnetism: 777 Nanoparticles and Thin Films, Oxford University Press, 2023.

- 778 87. R. Chantrell, J. Popplewell and S. Charles, *IEEE Transactions on Magnetics*, 1978, 14, 975 View Article Online 779 977.
- 780 88. D. Hawkins, D. Stevenson and S. Reddy, Analytica Chimica Acta, 2005, 542, 61-65.
- 781 89. E. Saridakis, S. Khurshid, L. Govada, Q. Phan, D. Hawkins, G. Crichlow, E. Lolis, S. Reddy and
 782 N. Chayen, *Proceedings of the National Academy of Sciences of the United States of America*,
 783 2011, 108, 11081-11086.
- 784 90. A. N. Stephen, S. R. Dennison, M. A. Holden and S. M. Reddy, *Analyst*, 2023, **148**, 5476-5485.

Simple Size Tuning of Magnetic Nanoparticles using a Microwave MADILITE Solvothermal Method and their Application to Facilitate Solid Phase Synthesis of Smart Polymers.

Andrei N Stephen¹, William Stockburn¹, Sarah R Dennison¹, Tim Mercer² and Subrayal M Reddy^{1*}

¹Department of Chemistry, Institute of Materials and Investigative Sciences, UCLan Centre for Smart Materials, School of Pharmacy and Biomedical Sciences, University of Central Lancashire, Preston, PR1 2HE, United Kingdom.

²Magnetic Materials Research Group, Jeremiah Horrocks Institute for Mathematics, Physics & Astronomy, University of Central Lancashire, Preston, PR1 2HE.

*Corresponding author: smreddy@uclan.ac.uk

Data Availability Statement

All data are available within the article and its Supplementary Information files and from the authors upon request.